Romanian Reports in Physics, Vol. 59, No. 1, P. 45–85, 2007

OPTICS AND QUANTUM ELECTRONICS

ULTRAINTENSE TABLETOP LASER ENGINEERING: EXCIMER AMPLIFIER STAGE

S. MARTELLUCCI[1], M. FRANCUCCI[1], P. CIUFFA[2]

[1] *University of Rome "Tor Vergata", Department of "Ingegneria dell'Impresa", Via del Politecnico n. 1, 00133 Rome, Italy*
e-mail: smart@uniroma2.it or francucci@ing.uniroma2.it
[2] *Elettronica s.p.a., Systems Technology and Processing Department, 00131 Rome, Italy*
patrizio.ciuffa@elt.it

(Received 24 July 2006)

Abstract. The advent of the Ultraintense Tabletop Laser Systems (UITLSs) has opened new and until then unexpected frontiers allowing the development and the progress of new research areas, in particular in scientific and industrial fields. Usually, these laser systems are used to generate plasma on solid or gaseous targets, so-called Laser Induced Plasma (LIP). The generated plasma behaves like a source of visible, UV and X radiation, that can be used for many applications. In particular, UITLSs are used for radiation−matter interaction studies, fundamental plasma parameter determination, astrophysical applications, inertial confinement fusion, studies in the high energy physics or in the compact particle accelerator field, quantum electrodynamics studies, industrial production processes concerning soldering, targeting, drilling, micromachining, etc. The UITLS designing and realization are very hard jobs that need of interdisciplinary cooperative efforts between researchers of different disciplines: physics, chemistry, engineering, material science, etc. In this paper, is explained an UITLS developing in Tor Vergata University laboratories: UV laser source (248nm / 50fs / 100mJ / max repetition rate = 100Hz) based on a Ti:Sapphire (Ti:Sa) crystal oscillator, CPA+MPA techniques and Excimer End Amplifier that will be treated in its design details and characterized.

Key words: laser, plasma, Ti:Sa, CPA, excimer amplifier, self-sustained electrical discharge, main discharge, preionizer, thyratron, protection circuit, DC-priming, heat sink, core inductor.

1. INTRODUCTION

In terms of international competition Japan, USA and Europe have recognized the potential of Microsystems in the late 1980's. Microsystems will increase competitiveness of products by lowering the manufacturing costs, by increasing the performances or both. Promising areas are of course mass markets like automotive and consumer products, that explain the amount of effort invested

in this field by large Japanese, American and European companies. The cost of Microsystems depends mostly on technology (number of steps) rather than effective complexity of fabricated device.

This is a new chance for small and medium sized creative companies. Completely new products can be imagined and lead to niche markets, where the European small and medium enterprises are competitive. Europe strengthens its position in this field investing in research and development interdisciplinary activities with industrial executives and R&D engineers groups. The article treats either a technological aspect or application fields and emphasizes the design practice and the theory.

2. APPARATUS DESCRIPTION (IN PROGRESS)

Tor Vergata ultraintense *fs* tabletop laser system (**λ=248nm**, max pulse energy $\boldsymbol{E_{max}}$**=100mJ**, final pulse duration **τ ≅ 50fs**, **Pulse Repetion Rate=100Hz**), based on Ti:Sa oscillator and that will work in pulsed regime using ultrashort UV laser radiation, is schematically represented in the next figure.

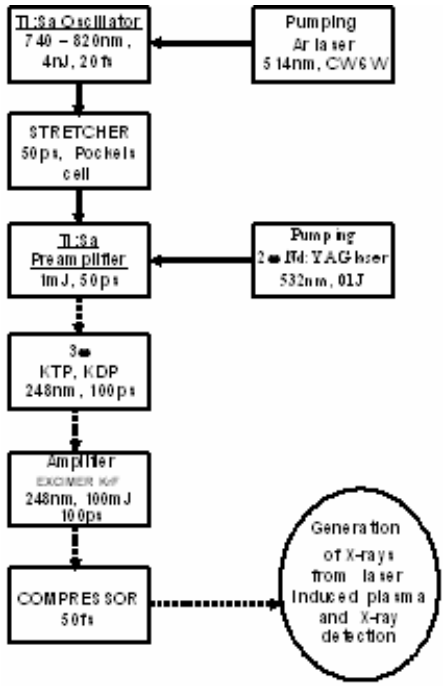

Fig. 1 − Scheme of the Tor Vergata *fs* Ti:Sa laser system based on the CPA technique and MPA architecture.

Our *fs* laser source is constituted through Ti:Sa oscillator, Argon pumping laser, stretcher, Pockels cell, multi-passage Ti:Sa preamplifier, another pumping laser (duplicated Nd:YAG laser), KDP or KTP crystals to triplicate Ti:Sa laser frequency, multi-passage Excimer KrF laser End amplifier, compressor and X-ray vacuum chamber.

Moreover, in the previous figure note that blocks, which represent various units of system, are connected through continuous or discontinuous arrows to evidence respectively units already working, tested and integrated in the system or units that alone work and usually have been tested, but not still integrated in our system.

KrF excimer laser [1] has been installed in our apparatus but actually is tested alone; when it will be inserted in the complete system, we expect to obtain laser pulses with the following characteristics: **λ=248nm**; ***energy E*=0.1J**; ***duration* τ = 100ps**; ***Pulse Repetion Rate* (PRR)=100Hz**.

After KrF excimer laser, radiation reaches **compressor** that acts on temporal duration of laser pulse to compresses it at initial value; practically, compressor doesn't make this exactly and laser pulse duration, after compressor, is always slightly longer than duration that laser pulse has after Ti:Sa oscillator.

Compressor is constituted through similar structure to stretcher and, practically, is complementary element of stretcher; it is not still integrated on our laser apparatus but, when it will be integrated, we expect to have laser pulse width equal to **50fs after compressor**.

3. THE EXCIMER AMPLIFIER STAGE

KrF excimer laser is used as end amplification stage of Tor Vergata *fs* laser source and has been completely designed, developed, realized in our laboratory; testing is almost completely done and, at maximum performance, has evidenced reliability problem with protection circuit toward External Trigger Module for thyratron, now in progress of resolution.

Before describing this end amplification stage, it is opportune to make some considerations concerning excimer laser physical principles.

The excimer laser is a gas laser that uses diatomic molecules. Two atoms, that form diatomic molecules, are bonded only when they are excited, while they are separated when molecules are not excited.

Often, one of two atoms (or both) is a **noble gas (Rare Gas)** that has high excitation energy (n*eV); in fact, first ionization energy varies from 12.1eV for Xenon to 24.6eV for Helium.

Then, it is obvious that generated radiation will be in the *UV* region (for example, Ar_2^* has λ=126nm, Kr_2^* has λ=146nm, Xe_2^* has λ=172nm). Other atom is normally **halogen gas** (**Halide** like F_2, C_2, etc…); in this case, we speak of excimers type **RGH**.

Using M_2 symbol for noble gas molecule and X symbol for halogen atom, laser transition happens between an excited level, in which ionic bond (strong and energetic) exists between M^+ and X^- ions, and repulsive or weakly attractive normal state, offered from covalent bond of type $M_2 + X$.

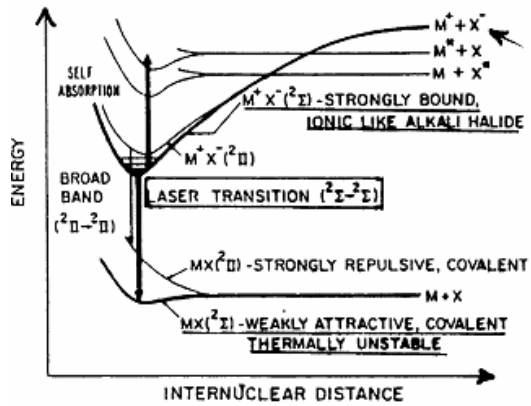

Fig. 2 − Potential energy of the electronic bond between excited dimer molecules *versus* internuclear distance.

By contribution of external energy, population inversion (n^*) is created between normal state (n_1) and excited state (n_2); generally:

$$n^* = n_2 - n_1 \leq n_2 \tag{1}$$

so active medium introduces high gain. Normally, potential energy of excimer molecule is the lowest between chemical species formed by electrical discharge. Successively, many of them transform to excimer molecule, losing energy through chemical reactions; all this justifies high conversion efficiency of excimer laser. The following table shows **RGH** excimers used in research and in industry fields:

Table 1

RGH excimers: parentheses *()* indicate only spontaneous emission (LED) and symbol □ indicates high efficiency stimulated emission (LASER)

	He E_i=24.58eV	**Ne** E_i=21.56eV	**Ar** E_i=15.76eV	**Kr** E_i=14eV	**Xe** E_i=12.14eV
F	-	(108)	193	248	351
Cl	-	-	(175)	222	308
Br	-	-	-	(206)	282
I	-	-	-	-	(253)

An excimer laser is realized by large toroidal hermetic chamber filled with two reagent gases (Kr and F, for example), to a pressure of some mbar, and with a third (noble) gas, with higher ionization energy (called **buffer gas**), loaded to a pressure of some atmospheres.

Practically, buffer gas absorbs energy from excitation source and allows two reagent gases to receive and use it for population inversion. It participates to first ionization of mixture that excites noble gas, forming ionic bond with halogen ionized by absorbing an electron at same time.

The excitation sources can be a large number and they are listed in the following table:

Table 2

Pumping sources and their complexity: pulse energy and repetition frequency

Pumping (or excitation) sources	***Pulse energy***	***Repetition frequency***
Electron beams	High	Low
Proton beams	Complicated	
Nuclear fission	Complicated (low efficiency)	
Radiofrequency	High	Low
Self-sustained electrical discharge	Middle	High

Tor Vergata KrF excimer laser amplifier contains pumping with self-sustained electrical discharge (main discharge), initialized by hard X-ray preionization. Active volume, interested to main discharge, varies from 0.1 to 10 liters and is comprised between two electrodes: anode, isolated from chamber chassis by means of plastic support; cathode, connected to ground, constituted as metallic grid that permits hard X-ray passage for preionizing the mixture. This one is placed in continuous recirculation by inner tangential large fan, activated by engine placed outside.

Main discharge energy, comprised between 10J and 10kJ, comes from an external circuit constituted by high voltage capacitor bench that accumulates energy before discharge command; then, by a gas switch (thyratron), closed in correspondence of preionization pulse command, and by a series inductance (external or parasite), main discharge pulse is formed temporarily.

The peak of discharge current pulse is of the order of (10− 100)kA and it is usually limited through mixture resistance in self-sustained discharge regime. Main discharge pulse duration varies normally from 50ns to 500ns and it is imposed from external oscillating circuit and discharge mixture.

Upper limit of 500ns derives from problem of discharge instability: after preionization, discharge is uniform; then, it will concentrate in conductive filaments (**streames**) where energy is dissipated in heat.

Therefore, it is opportune to impose low times of main discharge and, then, to wait some time for mixture relaxation in order to clean active volume between two discharges: passage of 3 active volumes after main discharge gives clean mixture for next discharge.

Concerning our KrF excimer laser amplifier, we consider **Wall−Plug total conversion efficiency** (η_{WP}) of electric energy absorbed from power supply and converted to energy of emitted laser pulse.

So, η_{WP} is divided in three parts: first part is represented by conversion efficiency, η_{cs}, between electric energy absorbed from power supply and stored in capacitors and that one dissipates in main discharge ($\eta_{cs}\cong 50\%$); second part is represented by conversion efficiency, η_{se}, between energy dissipated in the main discharge and real pumping energy that creates the excited excimer ($\eta_{se}\cong 10\%$); third part is represented by conversion efficiency, η_{el}, between pumping energy and total energy emitted from laser ($\eta_{el}\cong 40\%$).

Therefore, Wall – Plug total conversion efficiency **(η_{WP})** is equal to:

$$\eta_{WP} = \eta_{cs} \cdot \eta_{se} \cdot \eta_{el} \cong 2\% . \tag{2}$$

To make the modeling of volt-amperometric behavior at laser electrodes, shown from mixture working in self-sustained discharge regime, we consider simply XeCl excimer. In the discharge zone a plasma is created where, after some tens of *ns*, processes of electron production (due to Xe ionization) and electron loss (due to HCl presence) are balanced, giving place to the following continuity chemical equation:

$$\frac{\partial n_e}{\partial t} = \left(r_g - r_r\right) n_e = k_i\left[Xe\right] \cdot n_e - k_a\left[HCl\right] \cdot n_e . \tag{3}$$

where n_e is electron density, r_g and r_r are generation and recombination rates per volume unit respectively, k_i and k_a are reaction speeds of noble gas and halogen respectively, increasing with concentration, in partial pressure. Moreover, indicating with N the molecule number per cm^3 of solution and with ξ the average electric field, it is possible to introduce quantity called **specific electric field**, ξ/N, from which k_i and k_a depend; in particular, k_i is a monotone growing function of ξ/N quantity, while k_a is normally monotone decreasing. Electronic balance between generation rate (r_g) and recombination one (r_r) shows an **equilibrium point**.

Obviously, through state equation of perfect gases, we can explain volume concentration, N, of solution through working pressure, p, so specific electric field is transformable to equivalent quantity ξ/p. In addition, equilibrium point between generation and recombination rates is approximately reached after some tens of *ns* from beginning of main discharge; consequently, conditions of self-sustained electrical discharge have been reached and value of $n_e(t) = n_{e_{ss}}(t)$ remains constant respect to chemical reaction speeds, but variable respect to "slow" current supplied from main discharge circuit. Equilibrium point is characterized by precise value of

specific electric field $(\xi/p)_{ss}$: in order to know self-sustained voltage (V_{ss}) between two electrodes, one can use the following relation, where d is electrode distance:

$$V_{ss} = \left(\xi/p\right)_{ss} \cdot p \cdot d \ . \tag{4}$$

Note that, if n_e is constant, working voltage is about constant; one can write $V_l(t)=V_{ss}$ and, so, it is possible to consider analogy between laser and voltage ideal generator. Moreover, it is clear that buffer gas decides substantially N or p and therefore, through specific electric field of self-sustaining, electrode voltage necessary to mixture to absorb energy.

In the next equation, we report relations that permit to determine: a) electronic mobility, μ_e, in conditions of self-sustained electrical discharge, dependent on buffer gas and its pressure; b) self-sustained current density, $J_{ss}(t)$, by microscopic Ohm law. So, one obtains:

$$a)\ \ \mu_e \cong \frac{k_{BG}}{p} \qquad b)\ \ J_{ss}(t) = qn_{e_{ss}}(t)v_d \quad \Rightarrow \quad J_{ss}(t) = qn_{e_{ss}}(t)k_{BG}\left(\frac{\xi}{p}\right)_{ss} \tag{5}$$

where v_d is drift speed of charge carrier, q is its charge and k_{BG} is reaction speed of buffer gas (for example, k_{BG}=1 500 in the case of Neon).

Moreover, in the particular case of p_{HCl}=1.5torr and p_{Xe}=10torr, one obtains:

$$n_{e_{ss}}(t) = 5.4 \cdot 10^{12} J_{ss}(t) \ . \tag{6}$$

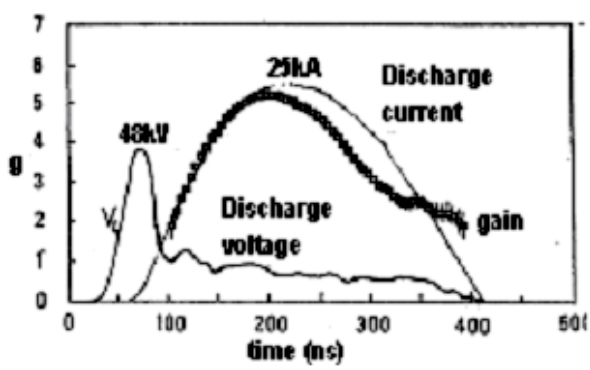

Fig. 3 − Voltamperometric behavior of gaseous mixture pumping regime *versus* time for XeCl excimer laser: voltage plateau makes evident the self-sustained phenomenon, V_{SS}, during the main discharge pulse.

Deposited power, $P_s(t)$, from main discharge circuit to mixture in conditions of self-sustained discharge, can be calculated by using the following relation,

where $W(t)$ is power for volume unit while ξ_{ss}, d, A, V_{ss}, I_{ss} are respectively electric field, electrode distance and area, voltage and current in self-sustained discharge conditions:

$$P_s(t) = W(t) \cdot d \cdot A = \xi_{ss} \cdot d \cdot J_{ss}(t) \cdot A = V_{ss} I_{ss}(t). \tag{7}$$

So, deposited energy (E_s) per pulse, τ_s, is equal to:

$$E_s = \int_0^{\tau_S} P_s(t)\,dt \cong \tfrac{2}{\pi} V_{ss} I_{ss_M} \tau_s \left[\frac{\mathrm{J}}{\mathrm{pulse}}\right], \tag{8}$$

where we have used sinusoidal approximation for discharge current, I_{ss}, with half period τ_s.

Consequently, pulse energy (E_L) emitted from excimer laser amplifier is obtained multiplying electric energy, E_s/η_{cs} , of power supply, for Wall–Plug total conversion efficiency **(η_{WP}),** that is:

$$E_L = \eta_{WP} \cdot \frac{E_s}{\eta_{CS}} \tag{9}$$

Therefore, energy of pulses emitted from excimer laser is comprised between 1mJ and 10J (in our case, we expect 100mJ), optimum for generating plasmas with electronic temperature, T_e, comprised between 10eV and hundreds of eV.

Moreover, it is important to observe that mixture, in conditions of self-sustained electrical discharge, corresponds to plasma characterized by a refractive index (r_p) and a wavelength (λ_p), that is:

$$r_p = \sqrt{1 - \left(\frac{\omega_p}{\omega}\right)^2} \qquad \Rightarrow \qquad \lambda_p = 2\pi c \sqrt{\frac{\varepsilon_0 m_e}{q \cdot n_e}}, \tag{10}$$

where ω_p, ω, c, q, ε_0 and m_e are respectively plasma frequency, laser frequency, light speed, carrier charge (for example electron charge), vacuum dielectric constant and electron mass.

Note that partial pressure design of mixture components requires satisfaction of $\lambda_{laser} < \lambda_p$. In addition, in the final part of half period (τ_s) of self-sustained electrical discharge, at the same time when filament formation begins, we can see a big increase of amplified beam divergence (from 0.1mrad to some mrad) in the orthogonal direction respect to propagation one and parallel to electrode surface.

These phenomena cause, former, the existence of a superior limit value in the halogen concentration and, on other hand, a limit value in the main discharge pulse duration (τ_s) and a more restrictive limit value in the current density of discharge peak, $J_{ss}(max)$. For example, when p_{Ne}=3bar and p_{Xe}=10torr, one obtains:

$$\left[HCl\right]_{\max} = 3\text{torr}; \qquad \left[HCl\right]_{opt} = 1.5\text{torr};$$
$$n_{e_{SS}}(t) < 10^{15}\text{cm}^{-3}; \qquad \tau_s < 400\text{ns}; \qquad J_{ss}(t) < 185\,\text{A}/\text{cm}^2. \tag{11}$$

3.1. APPARATUS DESCRIPTION

Following figure shows entire KrF excimer laser amplifier developed inside our laboratory of Tor Vergata University.

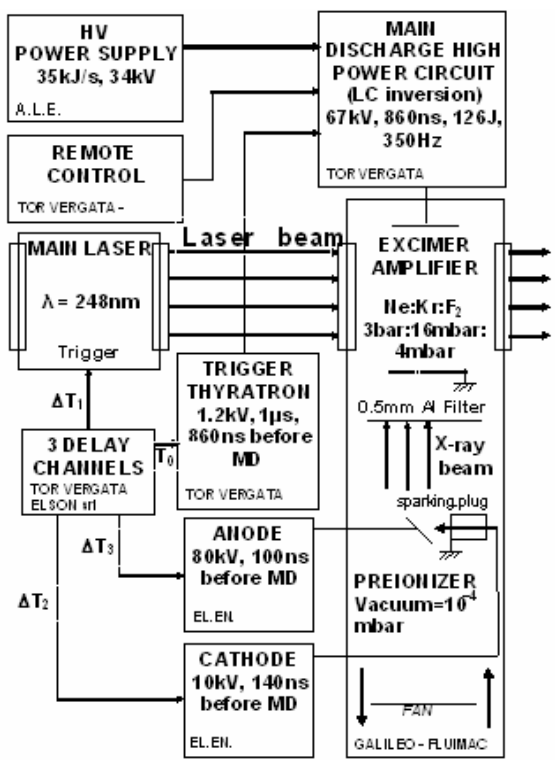

Fig. 4 − Functional block diagram of KrF excimer laser amplifier unit developed in the Tor Vergata research laboratory.

It is composed of a big hermetic chamber containing gaseous mixture for main laser pumping discharge, preionized by hard X-rays. We think to use Ne as buffer gas, at 3bar, and KrF as excimer (λ=248nm), with Krypton to the partial pressure of 16mbar and F_2 at 4mbar (0.1J, 100ps pulse at least). The discharge laser chamber is toroidal and has two discharge electrodes on the top (anode and grid cathode), where gaseous mixture circulates at high speed. On the bottom, a large tangential fan permits recirculation of gaseous mixture, moved by a strap-belt connected to a 14.7kW external triphase engine. Then an inside radiator, where circulates decalcified water, permits gaseous mixture cooling when we work at high pulse repetition rate of laser pulse (100Hz at least).

In the center, a preionizer is connected: a vacuum tube containing a large reflection diode, that generates hard X-rays toward upper gaseous mixture. Vacuum is obtained by diffusion pump driven in tail by a single stage rotative pump: value of vacuum is around 10^{-4}mbar.

Cathode is composed of a row of spark-plug, excited by an external high voltage pulse power supply (20kV); anode is a long metal bar, *45°* inclined in front of cathode, excited by an external very high voltage positive pulse power supply (90kV) able to attract cathode plasma electrons and reflect hard X-rays. Two tall rack holders contain the two preionizer pulse power supplies, based on thyratron switch and a pulse magnetic compressor obtained by a toroidal saturable transformer (from n*100ns to n*10ns). Such units have also an *INHIBIT* output that is used in order to block all local power supplies during the discharge phase. Instead, the second one contains the high voltage pulse current charger for supplying the Main Discharge power Circuit placed on the top of chamber.

MDC is inserted by a shaped electrode on anode of laser; an energy stored circuit is modulated to form MD pulse by a thyratron*, DC-primed* for minimizing jitter (<0.5ns). High power circuit (1kW at maximum PRR) is completely immersed in oil, recirculated by an external adjacent pump, to guarantee *PRR*≤ 350Hz. A Local Control Unit, containing lamp indication and protection circuit (automatic and manual), is realized in a remote control rack. Trigger driver for MDC thyratron comes from a rack unit realized in Tor Vergata laboratories (thanks to *E. Penco* and *R. Marchetti* technicians) based on a little thyratron that provides low jitter and fast inverse recovery time. An additional unit produces proper delayed synchronism pulses (source laser, cathode & anode preionizer, MDC) for aligning each laser unit, with delay available between 0μs to 16μs: first MDC pulse trigger, after 680ns cathode preionizer, after 40ns anode preionizer, after 180ns principal laser; doing that, the 100ps pulse train lies on maximum gain time interval of KrF excimer amplifier.

Fig. 5 − Image of the principal laser subsystem based on Ti:Sapphire oscillator and amplifier units. On the center-high it is possible to see Excimer Amplifier unit and on the right three rack systems for power supplies of the principal laser, excimer preionizer and excimer MDC.

3.1.1. Performances of Main Discharge chamber

Following figures show laser chamber infra-electrodes zone and circuit for modeling main discharge behavior respectively.

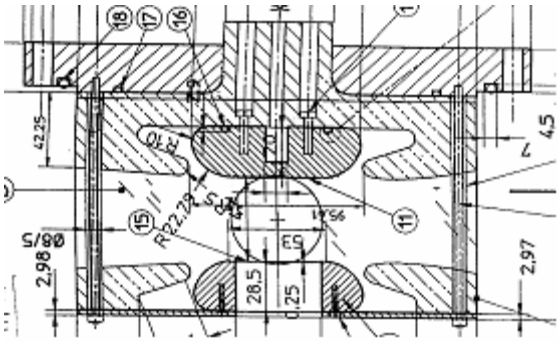

Fig. 6 − Mechanical design of the main discharge region, with laser nichelated aluminum electrodes and its plastic holders, developed by Galileo SpA.

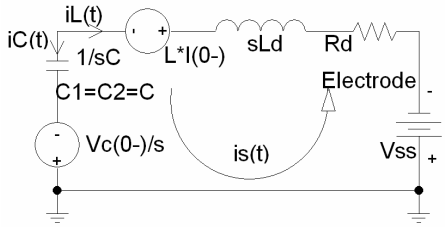

Fig. 7 − Laplace Transformation of the damped oscillating circuit for modeling Main Electric Discharge after thyratron commutation.

Hollow cathode with grid surface permits hard X-ray passage, and bulk anode (fixed on Plastic PVDF support) shows a back center tap line for MD electrical electrode insertion. Area is A=651cm^2, with lenght L=70cm and spacing is d=4.7cm. From previous paragraphs, values of voltage and current of self-sustained discharge are:

$$\begin{aligned} V_{ss} &= 10.86\text{kV} \\ I_{ss_M} &= 120.4\text{kA} \end{aligned} . \tag{12}$$

Maximum current of MDC and energy transferred to gas mixture can be estimated by solving equation of electrical dumped oscillating circuit: capacitors bench with equivalent capacitance C, parasitic resistance R_d and inductance L_d of discharge electrode, equivalent constant generator of mixture V_{ss}.

Equivalent capacitance C=56nF has initial condition $V_c(0^-)$=67kV and total stored electrical energy E_c=126J. Estimated value of L_d=30nH has initial condition $I_L(0^-)$=0A; R_d is estimated by modeling electrical electrode of MDC as a series of parallelepiped of length l_1=96.5cm, and trapezoidal copper part of l_2=141.5cm, and applying second Ohm law:

$$R_d = R_{upper} + R_{down} = \rho_{Cu}\frac{l_1}{S_1} + \rho_{Cu}\frac{l_2}{S_1}\frac{\ln\left(\dfrac{t_u/t_d}{w_u/w_d}\right)}{\dfrac{t_u}{t_d}+\dfrac{w_u}{w_d}} = 2.61\mu\Omega\,, \tag{13}$$

where $S_1 = l_1 t_u$ is electrode area, $t_u = t_d = 4$mm the thickness and w_u, w_d the width of trapezoid.

Analytical study gives for capacitance voltage:

$$I_L(s) + I_C(s) = 0 \quad \Rightarrow \quad V_C(s) = \frac{A + sE + s^2F}{s\left(1 + s\dfrac{2\delta}{\omega_n} + \dfrac{s^2}{\omega_n^2}\right)} \equiv \frac{A}{s} + \frac{B}{s-p} + \frac{B^*}{s-p^*}$$

$$\begin{cases} A = V_{ss} \\ E = V_C(0^-)CR_d - LI(0^-) \\ F = V_C(0^-)CL \\ \delta = \dfrac{R_d}{2Z_0} \\ \omega_n = \dfrac{1}{\sqrt{LC}} \\ Z_0 = \sqrt{L/C} \end{cases} \quad \begin{cases} B = \dfrac{A}{2}\left[\left(\omega_n^2F - 1\right) + i\dfrac{\delta}{\sqrt{1-\delta^2}}\left(1 + \omega_n^2F - \dfrac{\omega_n}{\delta}E\right)\right] \\ |B| = \dfrac{A}{2}\sqrt{\left(\omega_n^2F-1\right)^2 + \dfrac{\delta^2}{1-\delta^2}\left(1+\omega_n^2F - \dfrac{\omega_n}{\delta}E\right)^2} \\ \angle B = \arccos\left(\dfrac{\Re\{B\}}{2B}\right)\cdot \operatorname{sgn}\Im\{B\} \end{cases} \tag{14}$$

where δ is damping coefficient of circuits, ω_n natural angular frequency, Z_0 characteristic impedance.

By Laplace anti-transformation, time domain capacitor voltage is:

$$V_C(t) = A1(t) + 2|B|e^{\sigma}\cos(\omega t + \angle B)1(t)$$
$$\begin{cases} \sigma = -\delta\omega_n \\ \omega = \omega_n\sqrt{1-\delta^2}. \end{cases} \tag{15}$$

Now, by deriving capacitor current $i_C(t)$, evaluating its first stationary points, noting that δ≅0 (heavily underdamped circuit) and Z_0=0.73Ω, is obtained following self-sustained discharge peak current:

$$I_{ss_{peak}} = \frac{V_C(0^-) - V_{ss}}{Z_0} e^{-\frac{\delta \arccos\delta}{\sqrt{1-\delta^2}}} \cong 76.7\text{kA} < I_{ss_{MAX}}. \tag{16}$$

Duration of semioscillation of self-sustained discharge, energy transferred per pulse and consequently loss energy in successive oscillations are:

$$\begin{aligned} &\tau_s = \pi\sqrt{L_d C} = 129\text{ns} \\ &E_{ss} = \frac{2}{\pi} V_{ss} I_{ss_{peak}} \tau_s = 68.4\,\text{J/pulse} \Rightarrow E_{loss} = E_C - E_{SS} = 57.6\,\text{J/pulse} \quad (\eta_{cs} \approx 45.7\%) \\ &E_l = \eta_{sl} E_{ss} = 2.74\,\text{J/pulse} \quad \Rightarrow \quad P_l = PRR_{\max} \cdot E_l = 0.95\text{kW} \end{aligned} \tag{17}$$

due to the fact that laser pulse passes during first discharge oscillation and V_{ss} changes sign on each inversion of discharge current. Typical value assumed for conversion efficiency, between deposited energy and emitted laser energy, is η_{sl}=4%, and is used maximum PRR=346Hz (see later).

Finally, the small signal gain of amplifier stage is connected to excimer concentration, proportional to self-sustained discharge energy divided to pumping energy:

$$[XeCl^*] = \frac{E_{ss}}{h\nu} \frac{\tau_s}{\tau_{[XeCl^*]}} \eta_{se} = 1.37 \cdot 10^{14}, \tag{18}$$

where $\tau_{[XeCl^*]}$≅10ns is excimer lifetime. Since intensity is $I = n_f \cdot c \cdot h\nu$ and excimer disexcitation cross section is $\sigma_{f\text{-}e}$, one obtains:

$$\begin{aligned} &dI = n_f \cdot [XeCl^*]\sigma_{f-e} \cdot dz \\ &g \hat{=} [XeCl^*]\sigma_{f-e} = 1.37 \cdot 10^{-2}\text{cm}^{-1} \\ &G_1 = e^{NgL\left(\frac{\sqrt{\gamma}-1}{\gamma}\right)} = 1.86, \end{aligned} \tag{19}$$

with g = stimulated absorption small signal gain coefficient, N = number of passages = 3 p.e. and γ = small signal gain to absorption ratio $\cong 10$ for excimer. Lower lifetime of KrF* ($\tau_{[KrF^*]} \cong 3$ns) gives higher gain, but it is more unstable of XeCl*: for this reason we have reduced to τ_s=129ns duration of self-sustained discharge.

3.1.2. Preionizer performance

Preionizer is a second hermetic chamber located in the center of the toroidal discharge chamber that acts as a Roentgen vacuum tube, at 10^{-5} – 10^{-4} mbar, containing a large reflection diode that generates hard X-rays toward excimer gaseous mixture.

The preionizer cathode is constituted by a row of 25 sparking plug, driven by 0 to 25kV high voltage discharge pulse, 3μs duration and 100A / Sparking plug. Preionizer anode is constituted by a long bar, at –45° front of sparking plugs, where a very high voltage positive pulse is applied for attracting the cathode plasma electrons.

For bremsstrahlung, hard X-rays are reflected specularly at +45° toward MD electrode, by crossing a 0.5mm thick Aluminum filter that divides vacuum preionizer to high pressure MD chamber.

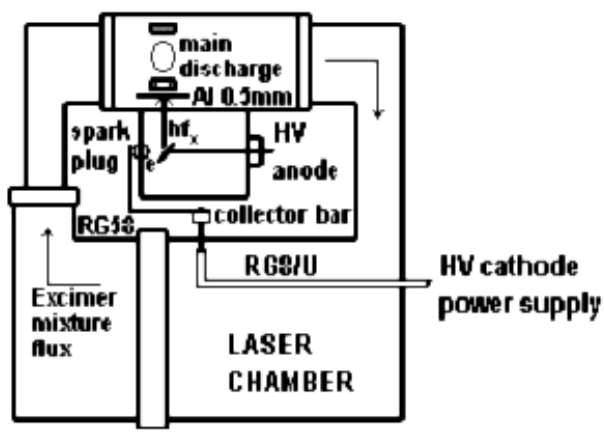

Fig. 8 − Drawing of the toroidal laser chamber with preionizer in the center.

When electron passes near a nucleus N can receive a fast deceleration, and emits electromagnetic energy. Well known is irradiated energy spectrum, $E(\lambda)$, as function of impact kinetic energy E_e that determines the minimum emitted wavelength components, that is $hf \leq E_e$. Hard X and γ-rays generators usually are based on bremsstrahlung mechanism. Volume spectrum density of photons, $N_{hf}(hf)$,

theoretically linearly decreases to null at maximum kinetic energy corresponding to anodic voltage, $E_{max}=V_A \cdot e$, and the peak frequency is at $E_{picco}={}^2/_3 V_A$. Due to anodic voltage not constant but pulsed, spectral density of hard X photons is less than linear and the effective peak will be at photon energy:

$$h\nu_{peak} \cong \frac{V_A \cdot e}{3}. \tag{20}$$

Next figure shows electric scheme of preionizer with explicative anodic pulse former based on a toroidal transformer that acts as a Pulse Magnetic Compressor from n*100ns to n*10ns; performances of pulse are: discharge energy=8J, τ_{FWHM}=60ns, V_A(peak)=90kV. We have used anodic peak voltage variable from 60kV to 90kV; so, obtained photon peak energy lies on the range 20keV to 30keV, where 0.5mm thick aluminum filter ($Al_{98.4\%}/Si_{1\%}/Mg_{0.6\%}$) has a transmissivity comprised in the interval T_{Al}(0.5mm, 20keV)=0.68 and T_{Al}(0.5mm, 30keV)=0.87.

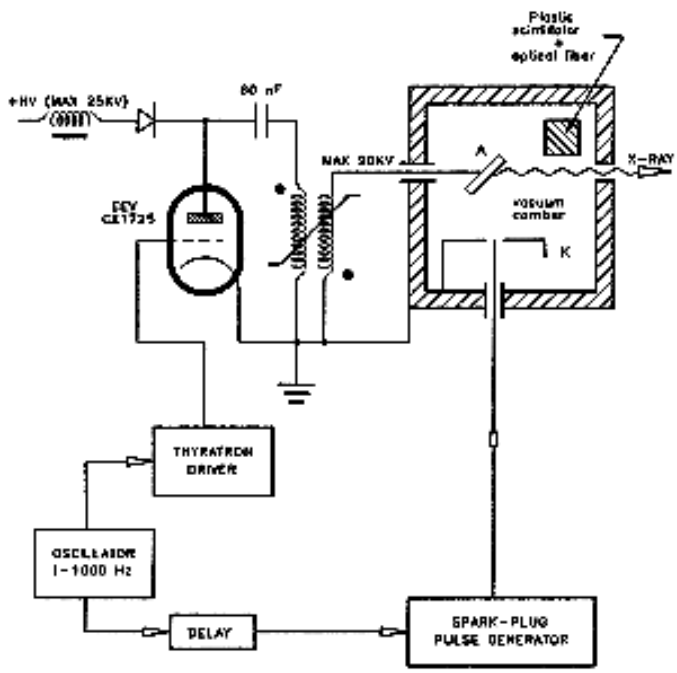

Fig. 9 − Spiker electric circuit for the preionizer anode based on a saturable switch toroidal transformer that acts as a Pulse Magnetic Compressor circuit; also shown are external modules representing pulse oscillator trigger, thyratron based standard driver for Anodic spiker, delayer and Spark-plug pulse generator for preionizer cathode.

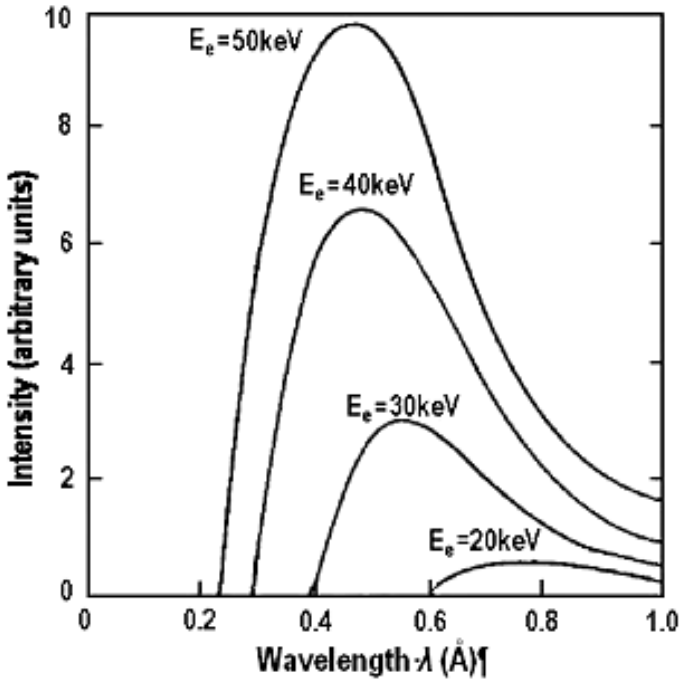

Fig. 10 − Hard X-rays energy spectrum emitted from the preionizer *versus* wavelength λ.

Preionizer anodic and cathodic discharge circuits are designed to operate at PRR_{MAX}=1kHz, with yet explained **recirculation factor** of gaseous mixture equal to 3. Cathodic spiker is able to source a maximum pulse energy of Ek_{MAX}=0.4J/pulse at a discharge voltage of maximum 25kV. This pulse is conducted by a 7m of RG8/U coaxial cable to collector bar of 0.4Ω parasitic resistance where current is divided into 25 almost equal parts, each ones composed of a capacitor in series to sparking-plug. This high voltage capacitor initially was obtained by a piece of L=43.5cm of RG58 coaxial cable with first plate given by central wire and second plate given by shield: total value is the product of lineic capacitance with L, that is $C_{RG58}=100^{pF}/_{m}\cdot L$=43.5pF. After 1 000 cathode shots, two of coax cables were fired, so we have substituted them with 50pF/40kV bulk capacitances, till now working.

The need for working with sparking plug series capacitance (with parasitic resistance and inductance of wiring) becomes from aim of decoupling and equalizing energy and current discharge of each spark-plug: that is, avoid commutation of faster spark-plug that compromises the others.

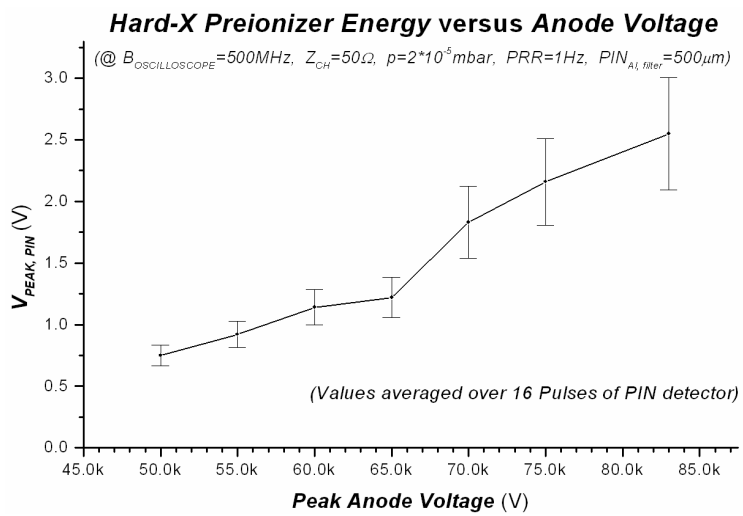

Fig. 11 − Graph illustrating experimental measurement of hard X-rays energy of Tor Vergata preionizer by using PIN photodiode sensor exposed, without filter, directly on cathode grid of laser head, inside 4.7cm spacing. Ordinate reports PIN peak voltage pulse, so energy will be obtained in future by integrating over spectral transmittance of $Al_{0.5mm}$ filter, spectral responsivity of silicon PIN sensor, spectral emission of Roentgen tube and geometric attenuation of surface of laser head cathode electrode.

Commutation dissipation energy, E_{SP}, equals capacitance stored energy, E_C, during cathodic pulse period; so, by using cathodic discharge pulse of V_K=10kV, is obtained the energy totally discharged on 25 spark plugs:

$$E_C = \frac{1}{2} C_{RG58} V_K^2 \cong E_{SP} \Rightarrow E_K = n_{SP} \cdot E_{SP} \cong 54.4 \text{ mJ/pulse}. \tag{21}$$

3.2. MAIN DISCHARGE HIGH POWER CIRCUIT (MDC)

We have seen that MD energy comes from an inside MDC capacitor of equivalent value C=56nF, precharged at V_C=67kV with E_C=126J. Actual scheme of MDC is composed of a high voltage and current circuit, called Modulator, and a medium voltage and current circuit consists on two PCB and sparse components, for modulator biasing. LC-inversion modulator configuration provides two series sections of discharge capacitance, C_1 and C_2, with extremes connected to laser head electrodes, and central tap to HV switches.

During charging long period (~12ms), the series R_m and L_m puts in parallel C_1 and C_2 that can be charged at maximum value of V_C=33.5kV by R_t and L_o path. When thyratron is driven to switch-on, an oscillation circuit is composed by C_2, external discharge inductance L_o and its parasitic resistance R_o, parasitic series inductance L_{thy} and self-sustained discharge constant voltage V_{SS}(thy)≅100V of thyratron.

Damping coefficient is δ≅0, so C_2 voltage is almost perfectly inverted in ½ period of oscillation, which is around 860ns, and sums absolutely with V_{C1}. In this time, laser head voltage is going from V_l=0V to V_l≅-67kV and now it's time to preionize gaseous mixture for starting self-sustained main discharge for excimer laser pumping.

Big EEV CX1725 thyratron, before triggering, is opened circuit, able to sustain more than 40kV static voltage; after triggering, L_{thy} causes partitioning of C_2 voltage and input line is exposed to negative $V_{in} \cong -6$kV, hazardous for HVPS.

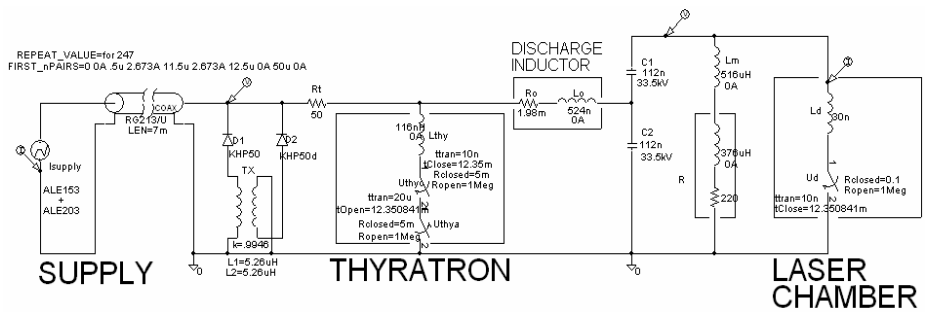

Fig. 12 − Electric scheme of Tor Vergata Main Discharge Circuit modulator, realized in LC-inversion configuration, and simulated by SPICE.

This problem is overcome by input protection clamp network, composed by two KHP50 High Voltage diodes and common mode transformer, TX, for equilibrating protection diode currents, that fixes negative pulse to $V_{in} \cong$ -90V.

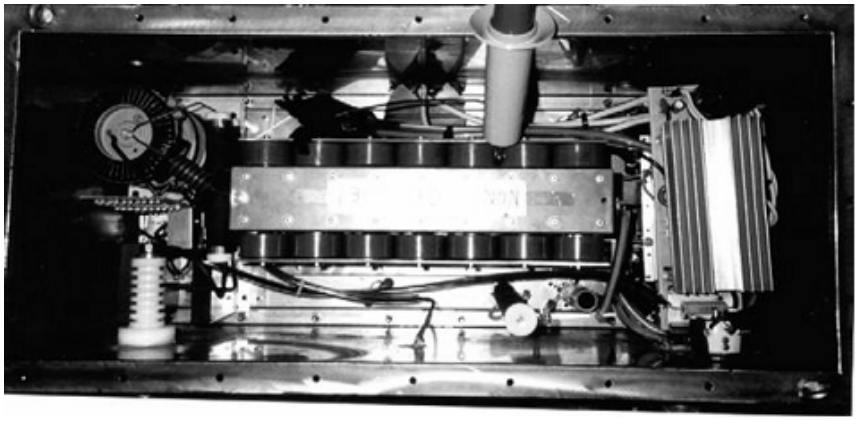

Fig. 13 − Photo illustrating inside top view of Tor Vergata Main Discharge high power circuit connected to laser head electrodes. In the center, capacitors bench; on the left, Thyratron, grid biasing high voltage PCB, HVPS input protection circuit; on the right, high power low voltage PCB for filaments biasing. This is for DC-Priming of thyratron.

8878 BELDEN high voltage 50Ω - 7m coax cable connects external HVPS to MDC: during charge current pulse, this line is terminated to proper R_t=50Ω through L_o, C_1 and C_2. Then, R_t dissipates protection energy due to protection input diodes, at max PRR=350Hz: this justifies its realization by two 100Ω parallel wired resistors. During C_1 charging, series L_m and R_m is designed for a damping factor δ≅1, fast and without oscillation. R_m is a single plane wired resistor, with parasitic inductance L_{Rm}=376μH, so L_m is only 516μH. All circuit is immersed in oil with high dielectric rigidity (>60kV/cm) and high thermal conductibility, with oil recirculation system.

3.2.1. Discharge capacitors bench

Capacitor bench is composed of 4 arrays of 28 capacitors each, with two external ground electrodes for C_2, a mid U-shaped electrode for C_2 - C_1 connection, and the central electrode of C_1 connected directly to anode of laser head electrode for Main Discharge.

Respect to older $BaTiO_3$ type, low loss is important at maximum PRR=350Hz and low piezoelectric effect, of about $\Delta C \leq 10\%$, implies a little reduction of capacitance at voltage near to nominal maximum. But the best performance is the reduction in Failure Rate that increases capacitor lifetime MTTF=$^1/_{\text{FAILURE RATE}}$. Finally, it exhibits low parasitic electrode inductance due to large cross-section of electrodes, well estimated by following relation:

$$L_{par.} \cong \frac{\mu_0}{2\pi} l \ln \frac{d+r}{r}\bigg|_{d+r=l} \cong 10\text{nH}, \tag{22}$$

obtained considering a spice of straight conductor of radius r and length l and an external confinement of magnetic induction B at a distance d experimentally verified at value l–r.

3.2.2. High Voltage power Supplies for MDC

HVPS for MDC is composed of two current pulse high voltage generators that need to close on a capacitor load: the first is master and second slave.

Outputs can be put in parallel and a hydraulic series circuit heat sinks both generators. Average power drawn from such current pulse HVPS rises linearly with voltage set on master and assumes the value, at V=33.5kV, of P_{out}=P_{master}+P_{slave}=19.2kJ/s+25.6kJ/s = 44.8kJ/s. So, time T_C required to charge total capacitance C is given by ratio of energy stored E_C and P_{out}:

$$T_c = \frac{\frac{1}{2} C V_{out}^2}{P_{out}}, \tag{23}$$

where C is the sum of 112 capacitances of discharge bench, C_S=224nF, coaxial cable C_o=98pF/m·7m=686pF, internal capacitance of HVPS, C_a=400pF; so C=225nF and T_C=2.81ms. For evaluating maximum PRR of laser we have to sum T_C to MD duration, T_S≅4μs, thyratron recovery time, T_{rr}≅20μs, delay of inhibit readiness for disabling HVPS during MD, T_i ≅60μs, obtaining minimum time needed for MD that results T_{MD}≅2.894ms, so

$$PRR_{\max} = \frac{1}{T_{MD}} = 345\text{Hz}, \tag{24}$$

so PRR_{MAX} of laser is substantially decided by P_{out} of HVPS and total capacitance C_S of MDC bench, that is limited by physical systems volume.

Structure of HVPS, used for MDC, is a half controlled bridge AC/DC converter, with inductive output and $f_{SWITCHING}$=20kHz: output appears as current generator with voltage feedback stabilization, and with current pulse of constant duty of 25%.

Output power of HVPS is given by product of reached constant voltage, V_{out}, and *rms* value of drawn current, formula that permits to evaluate current pulse amplitude for simulation:

$$I_{eff} = \sqrt{\frac{1}{T}\int_0^{\tau} i_{out}^2(t)\,dt} = \frac{I_{\max}}{2} \quad \Rightarrow \quad I_{\max} = \frac{2 \cdot P_{out}(V_{out})}{V_{out}} = 2.7\text{A}\,. \tag{25}$$

3.2.3. Thyratron based High Power Switch

Paschen law asserts that a gas, at pressure p between two electrode spaced d, exhibits a breakdown voltage V_s function of product pd.

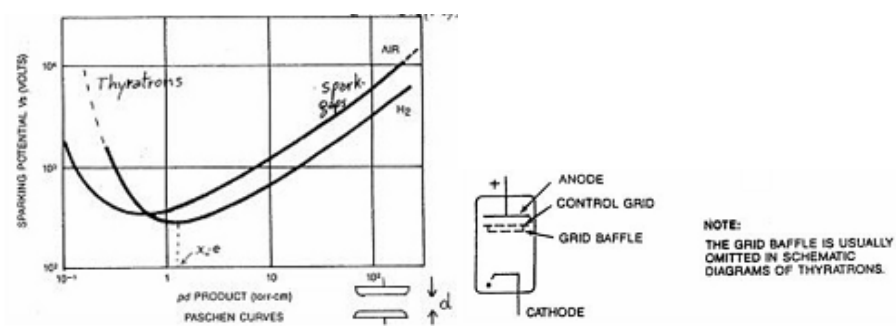

Fig. 14 − Graphs illustrating Paschen law for an air filled Spark Gap compared with an Hydrogen Thyratron: Paschen Minimum for hydrogen is 273V with $(pd)_{min}$=1.15torr·cm. Paschen law applies for plates and grids of thyratron: $V_S = V_{\min} \dfrac{pd/(pd)_{\min}}{1+\ln\left(pd/(pd)_{\min}\right)}$, where $(pd)_{min}$ is depending on gas used.

Typical thyratron, shown in previous figure, has anode and cathode extreme plates separated by a control grid, baffled for don't putting in sight anode and cathode. Then, *pd* for anode-grid pair is 0.1torr·cm, with high sparking voltage, instead *pd* for grid-cathode pair is at Paschen minimum, with discharge voltage reduced additionally by a hot cathode with thermoionic electrons region. So, thyratron is easy triggerable device: first, on applied positive grid-cathode voltage trigger, cathode electrons go toward grid and begin to ionize this gas region, forming plasma; then, plasma propagates toward very high positive voltage anode plate, forming a dense plasma in anode-grid region; finally, this plasma front propagates toward cathode via breakdown of gas, closing anode-cathode thyratron switch.

Time between trigger pulse and thyratron switch-on is called anode delay time, usually 100-200ns: it can be reduced by equilibrating/adjusting concentration of gas into thyratron during life or particular application, against trap state of electrodes surface, riequilibrating performance by varying voltage of additional cathode filament called reservoir. We have implemented that, in MDC, by a high power potentiometer on primary of high power transformer, but without exceeding to don't reduce voltage isolation of anode-cathode region. After commutation, thyratron is in self-sustained discharge and shows a voltage drop constant of 100-150V.

The opening of thyratron (reverse recovery) consists on neutralization of positive ions (the last because heavy carriers) on metallic surface of electrodes, implies a queue time T_{rr}=20-200μs (H_2 more light of D_2). So, Maximum PRR can't exceed inverse of T_{rr}. Recovery can be optimized by applying a negative voltage on control grid and/or anode plate after conduction phase, or by limiting rise time of aperture anode voltage.

Table 3

Comparison of performances between various high power switches for excimer laser applications

DEVICE	*ACTIVE MEDIUM*	*ANODE VOLTAGE*	*PEAK ANODE CURRENT*	*ANODE VOLTAGE RANGE*	*PRR* ($\cong 1/T_{rr}$)
Thyratron	Gas	70kV	20kA	≅100%	1kHz
Spark-Gap	Gas / Vacuum	100kV	100kA	≅10%	50Hz
Tiristor	Solid State	3kV	10kA	≅100%	10kHz
GTO	Solid State	3kV	10kA	≅100%	100kHz

Characteristic parameters of thyratron have data sheet limitations: this permits to verify and design external components of modulator and trigger circuit and maximum voltage of HVPS. So, we **consider our thyratron CX1725**. Supplier gives maximum peak repetitive anodic current i_{Apeak} and time interval T_p for it: so, total maximum pulse charge can be $Q_{pmax}= i_{Apeak}\cdot T_p$=15kA·0.5μs=7.5mC. Since anodic discharge current is sinusoidal, by choosing a conservative peak value of 14kA, from charge limit, we obtain the semiperiod of oscillation realized and external inductance:

$$T_p = \frac{Q_p}{i_{A_p}\frac{2}{\pi}} = 841\text{ns} \quad \Rightarrow \quad L = L_{thy} + L_o = \left(\frac{T_p}{\pi}\right)^2 \frac{1}{C_2} = 640\text{nH}. \tag{26}$$

The component of inductance due to thyratron, L_{thy}, can be estimated as in previous chapters, with calculation of negative input pulse:

$$L_{thy} \cong \frac{\mu_0}{2\pi} l \ln \frac{d+r}{r}\bigg|_{d+r=l} \cong 116\text{nH} \quad \Rightarrow \quad V_{neg.} = V_{C_2}\left(0^-\right)\frac{L_{thy}}{L} = -6.072\text{kV} \tag{27}$$

due to inductance divider, hazardous for external HVPS; $V_{C2}(0^-)$ is initial charging value. So, an input protection circuit is needed for clamping negative pulse (see later). To avoid damaging of thyratron plate, rate of rise of anode current can't exceed 300kA/μs, and not even average current exceed value of 5A:

$$\frac{\partial i_A}{\partial t}\bigg|_{\max} = \frac{V_{C_2}\left(0^-\right)}{L} = 52.3\frac{\text{kA}}{\mu\text{s}} < 300\frac{\text{kA}}{\mu\text{s}} \Rightarrow i_{A_{rms}} = \frac{2}{\pi} T_p PRR_{\max} i_{A_{peak}} = 2.62\text{A} < 5\text{A} \tag{28}$$

Finally, a good estimation of thyratron power dissipation is the sum of filament heaters and 200W per absorbed average ampere at PRR_{MAX}:

$$P_{thy_{MAX}} \cong P_{heater} + 200\frac{\text{W}}{\text{A}_{\text{AVE}}} \cdot i_{A_{AVE}} \le 800\text{W} \tag{29}$$

well dissipated by our structure totally immersed in oil.

3.2.4. Inductor measurement technique

All inductances calculated in this work and realized in various appropriate technology, according to levels of currents and/or voltages, are measured an then trimmed by a circuit meter based on series resonance, by varying frequency of 50Ω generator for minimum voltage on a time calibrated oscilloscope for measuring, along many periods, resonance angular frequency ω. A load resistor R=1kΩ, and formula $L_X=(\omega^2 \cdot C_X)^{-1}$ need.

3.2.5. Main discharge inductance

Power inductance for LC-inversion, placed in series with thyratron anode, has been realized in air for many reasons: avoid non linear effect on autoinduction coefficient introduced by ferromagnetic core, extremely high value of peak current, 14kA, that corresponds to very high magnetic field H that puts in saturation ferromagnetic core. A PVC support acts as holder of coil. **Nagaoka** formula justifies deviation from infinite solenoid:

$$L_{Nag.} = 4 \cdot 10^{-6} \pi^2 n^2 d \cdot F\left(\tfrac{d}{l}\right) \le L_\infty = 4 \cdot 10^{-6} \pi^2 n^2 d \cdot \left(\frac{d}{40l}\right), \tag{30}$$

where n number of loops, d inner diameter of support, l length of solenoid, $F(^d/_l)$ Nagaoka coefficient evaluated from standard graph.

Fig. 15 − Photo illustrating Tor Vergata power inductor for LC-inversion in series with thyratron anode, L_o=524nH; final computation has given, with d=23mm, l=40mm, loop spacing d_S=3.87mm, F=0.0116: $n_{Lo}\cong 7$ turns. Spacing d_S is needed for maintaining electrically isolated the loops with a proper thickness of oil. Measured inductance is 537nH.

The big cross-section of painted copper wire, ϕ=2.4mm, has been requested for reducing wire loss on total length of l_F=0.521m:

$$R_o = \rho_{Cu}\frac{l_F}{\pi\frac{\phi^2}{4}} = 1.987\text{m}\Omega \tag{31}$$

that provides a voltage fall of 28V at peak anodic current of 14kA.

3.2.6. Precharge circuit with bench HV inductor

Series R_M and L_M on modulator circuit provides precharge of capacitance section C_2 before main discharge on laser electrodes and has to be an quasi-open circuit on MD short pulse. These two devices have wire coil realization with large length and number of turns for minimizing voltage drop between closer turns when 67kV main discharge voltage pulse appears at laser head. R_M=220Ohm has parasitic inductance of 376μH, so L_M=516μH. Realization of L_M is only in air for maintaining low the inter-turns high voltage and to manage high pulse current of 41.2A during MD. Nagaoka formula is used with a correction term that takes into account the two floors of turns needed; used technique is called **bench inductor** because turn of second floor is wound on the last two turns of first floor. The right diameter of inductor is $d=\phi+\phi_S$, where ϕ=0.63mm is wire diameter and ϕ_S=25.9mm

is diameter of PVDF plastic coil support; length of entire closed loops coil is $l = 126$mm, $s = 1.86\phi$ is distance between closer loops, $B(^l/_s)\cong 0.33$ is correction factor from standard table. So:

$$L_M = 4\cdot 10^{-6}\pi^2 dn^2 \cdot F\left(\tfrac{d}{l}\right) - \frac{0.63n^2 d\left[0.693 + B\left(\tfrac{l}{s}\right)\right]}{\left(\tfrac{l}{s}\right)}\cdot 10^{-6}. \tag{32}$$

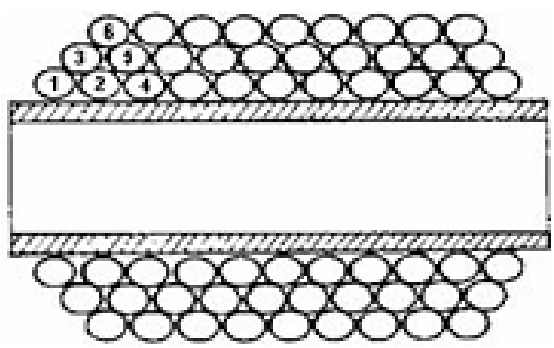

Fig. 16 − Drawing illustrating Tor Vergata precharge inductor L_M realized with bench technique, for a high voltage inductor. Two or more wire floors are not singularly wound but they are all gradually wound; so, discharge problem between closer turns is resolved. Spice presimulation of modulator has indicated I_{LM}=41.2A, fact that has carried out an air realization.

Number of turns for first floor has been n_1=194 and for second n_2=193. By this technique, maximum inter-turn voltage results between three closed turns, V_{SP}=448V, and it is much lower than electric rigidity of painted copper ≅6kV measured statically.

3.2.7. Input protection circuit

Input protection circuit of MDC is composed of two diodes KHP50 with very high reverse breakdown voltage, V_{BD}=50kV, paralleled with a common mode transformer designed in our Tor Vergata labs. Negative pulse puts in conduction diodes that fix it at forward voltage drop V_{AK}=84V.

Each HV diode is realized with a long series of matched Si diodes, so for SPICE simulation we introduce a model of a series of n equal diodes:

$$V_\Sigma(i) = n\cdot V_T \ln\left(\frac{i}{I_s}+1\right) \qquad \Rightarrow \qquad i = I_s\left(e^{\frac{V_\Sigma}{n\cdot V_T}} - 1\right) \tag{33}$$

where i and V_Σ are provided by supplier, through which we obtain $n = 208$ and $R_\Sigma = 0.1\Omega$.

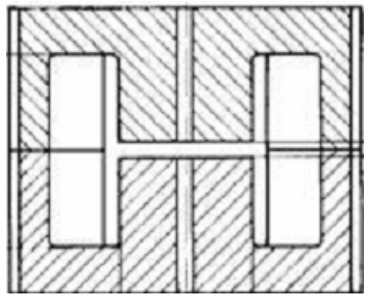

Fig. 17 − Common Mode Transformer with coil designed and carefully realized in our Tor Vergata labs; it is needed for High Voltage diodes for MDC input protection. At operative peak current, forward voltage is fixed to V_{AK}=84V according to measured value of 90V; from data sheet of diodes, I_{FSM}=300A, I_{AVE}=2.25A.

Common Mode Transformer (TMC) is introduced for dividing equally diode currents during input negative transient, for preventing avalanche destroying effect from one diode to the other. Model consists on making a linear transformation from diode currents I_1 and I_2 to the two differential and common components, I_c and I_d; so, common and differential mode inductances and ergo Common Mode Input Rejection Ratio are:

$$\begin{cases} L_c = L(1-k) \cong 39.6\text{nH} \\ L_d = L(1+k) \cong 10.5\mu\text{H} >> L_c \end{cases} \Rightarrow \quad CMIRR \triangleq \frac{L_d}{L_c} = 265 \ (\approx 48.5\text{dB}). \tag{34}$$

Each inductance, L_c, L_d, L=5.26μH, has been measured experimentally, so it has been possible to determine the layout quality parameters, k and I_{dMAX}, carefully obtained:

$$k = \frac{L_d - L_c}{L_d + L_c} \cong 0.9946; \quad I_{d_{MAX}} \cong \frac{V_{in_{MAX}}}{2R_t} = 60.1\text{A}. \tag{35}$$

The second formula indicates peak protection current in a single diode, as limited by 50Ω resistance, terminating input of MDC. Diode power dissipation is about 1W at maximum PRR. Simulation and measurement have been done by imposing dispersion in diode parameters, such as I_{S1}=2·I_{S2}, and TMC has virtually shown a differential drop of 2kV>>V_{AK} sorting the perfect equilibration of diodes currents, instead common voltage drop is negligible.

3.3. PCBS FOR FAST DC-PRIMING THYRATRON DRIVING

Two medium power Printed Circuit Boards have been designed and realized in our labs for DC biasing all grids of thyratron: technique called ***DC-Priming***.

Advantages are: lowest anode delay time, lowest reverse recovery time, lowest commutation jitter. Vice versa, designing is very difficult and carefull, with need of high level of integration in a "small" stainless steel box.

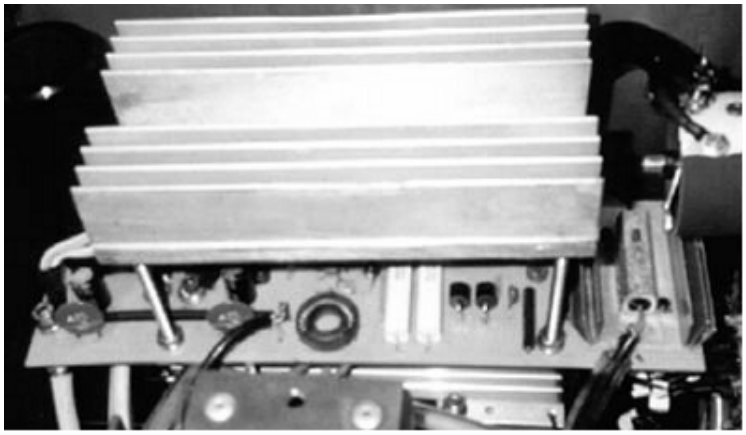

Fig. 18 − First of two Tor Vergata PCBs for DC-Priming of thyratron. Circuit is developed in various physical layers: on the center, PCB with medium power components for DC-supply of grids and the two cathode and reservoir filaments; on the top, heat sink for discrete Graetz bridge of cathode Schottky diodes; on the bottom, heat sink for reservoir Graetz bridge. Under these, the three transformers for mentioned DC-supplies: two for cathode and reservoir, the third is an insulation transformer for grids.

3.3.1. Triggering module for thyratron control

Rack of triggering module for thyratron control grid has been designed in Tor Vergata labs and realized by ELSOM SrL company.

It is based on smaller thyratron, CX1172, due to less jitter, one order lower of equivalent solid state devices: 5ns rise time jitter measured for solid state EG&G module TM29 and 0.5ns for our CX1172 based driver; additionally, fall time jitter is 30ns for together.

Model used for simulation is the series of: pulse waveform generator with open circuit piecewise approximation, a non linear output impedance well approximated by an exponential law.

So, by measurements, at $t = 0$s, rise time is 19ns with voltage reaching 1.15kV, then a tilt toward 766V, then falling to 0V at $t = 0.9$μs with pulse width PW = 0.5μs.

Series impedance model has been obtained by technique of varying an output resistive load: behavior is analogous to high threshold silicon diode (with high n):

$$\begin{aligned} & i_{CX1172} = I_s \left(e^{\frac{\Delta V_{OUT}}{n \cdot V_T}} - 1 \right) \\ & I_s = 2.32\text{A} \\ & n = 5\,500. \end{aligned} \tag{36}$$

Simulation has been in accordance with experimental results for grid voltages behavior and for our driver CX1172 at input connector of MDC.

3.3.2. Electric scheme of two PCBs for Thyratron DC-priming biasing

Following electric scheme contains a simple spice Thyratron model and electronic circuits realized on two PCBs for DC biasing of grids and filaments.

CX1725 is a 5 grid thyratron: anode plate and cathode plate, with its two heating filaments, control grid G2 for triggering, auxiliary grid G1 that creates the confined plasma region near cathode zones by its DC negative potential, gradient grid G3 that maintains constant the gradient of voltage (electric field) inside hydrogen tube by applying half of anode - cathode voltage for avoiding premature discharge.

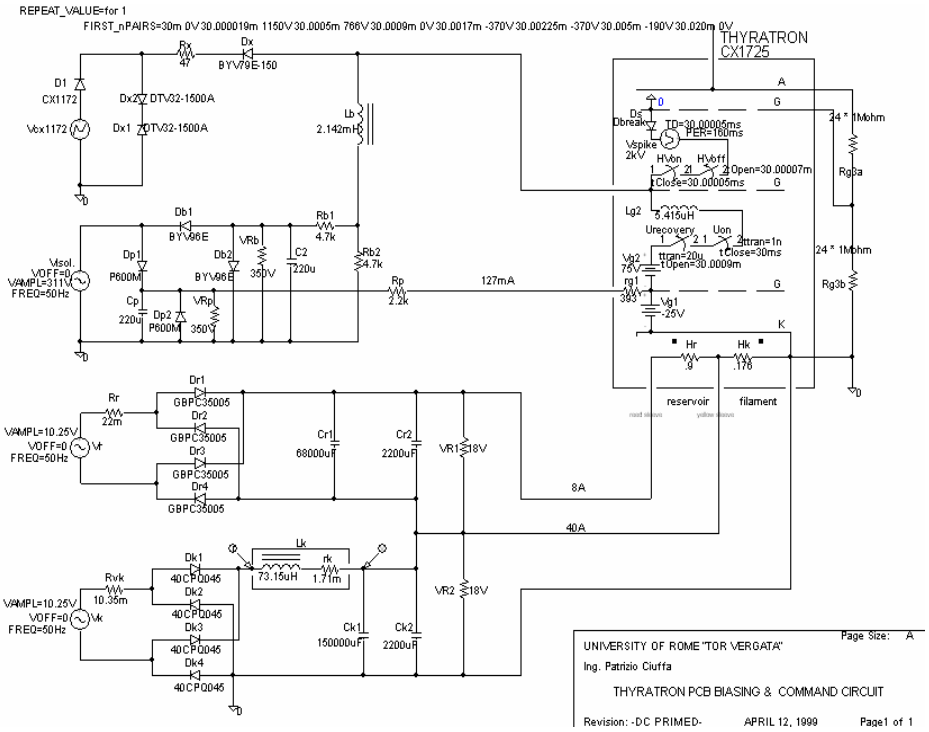

Fig. 19 − Electric scheme of two Tor Vergata PCBs for thyratron DC-Priming: first PCB contains two supplies for cathode and reservoir filaments, plus auxiliary and control grid supplies; second PCB contains the row of 24+24 gradient grid resistors, plus control grid input protection and adapting devices.

So, PCB placed along thyratron has 24+24 resistors of 1MΩ/2W/700V_{DC} for biasing **gradient grid** at $V_{AK}/2$ and reaching proper rigidity divider. Measurements of I/V characteristics on **auxiliary grid** have given a straight line ohmic behavior,

$V_{g1}= v_{g1}+ r_{g1}\cdot I_{g1}$ with intercept $v_{g1}= -25$V and slope $r_{g1}=393\Omega$: reason of negative intercept is that G1, close to cathode plasma, has shown the negative potential of spatial charge respect to positive cathode depauperated of electrons. External auxiliary grid current is chosen on the average of data sheet value, $I_{g1}=127$mA: this current is provided by an insulation transformer followed by half wave rectifier given by D_{p1}, C_p, D_{p2}, V_{rp1}, R_p; capacitance is designed to give following mean value and ripple, at aux grid current:

$$\begin{cases} V_m = 305\text{V} \\ V_r = 6\text{V} \end{cases} \quad \Rightarrow \quad C_p = \frac{I_{G1}}{n \cdot f \cdot 2V_r} \cong 212\mu\text{F}, \tag{37}$$

where n (=1) corresponds to number of half waves.

Varistor V_{rp1} is of type SIOV-S07k275 of 375V_{DC}/21J/0.25W and it protects from spurious commutation spikes coming from thyratron aux grid; R_p=2.2kΩ/50W/1.25kV is a metal case resistor dissipated on hand made and designed three layer heat sink, that provides aux grid biasing constant current. The pulse current of D_{p1} can be evaluated by pulse current of generic full wave rectifier:

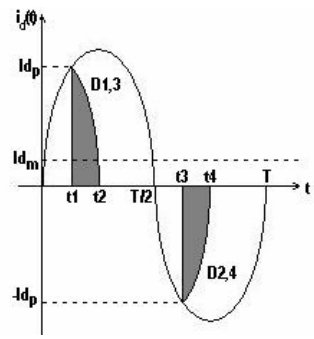

Fig. 20 − Waveform of pulse current in a generic full wave GRAETS bridge, when input sine voltage overcomes stabilized DC voltage of capacitor output filter.

Assuming that, in interval t_2-t_1, charge Q_d through diodes goes on filter capacitor and must be equal to charge Q_c that it delivers to load on successive time:

$$I_{d_p} \cong \frac{I_{d_m} \frac{\pi}{n}}{\sqrt{\frac{V_r}{V_p}}}, \tag{38}$$

that for aux grid provides: $n = 1$, I_{dp}=3.33A, used diode is P600M with I_{RPM}=6A and reverse maximum repetitive voltage V_{RRPM}=1kV.

Biasing circuit of control grid provides a negative voltage of V_{G2}=−150V needed for avoiding propagation of preformed cathode plasma. So, D_{b1}, C_b, D_{b2}, V_{rb1}, R_{b1}, R_{b2}, L_b, realize a half wave rectifier with following characteristics:

$$\begin{aligned} &V_{b_m} = -306\text{V} && I_{d_m} = 74\text{mA} \\ &V_r = 6\text{V} && I_{d_p} = 2.3\text{A}. \\ &V_{G2} = -149\text{V} \end{aligned} \tag{39}$$

Diodes are of type BYV96E/1000V/1.5A/300ns; ceramics R_{b1}=R_{b2}=4.7kΩ/17W are air heat sink and conduct, actually, a lower I_{dm}=35.6mA: with control pulse and at maximum PRR, we have a higher value of I_{dm} by current contribution through L_b. Inductor L_b is designed assuming that, with control pulse V_{G2}=(1kV, 1μs), the linearly rising i_{Lb} doesn't reach quiescent I_{dm}.

We have obtained L_b=2.14mH, possible by a toroidal ferrite core type R25. An 220V/160W **insulation transformer** is used for supplies of control and aux grids and to put the secondary to PCB ground, realizing two half wave rectifiers.

Part of circuit that transfers voltage from **external trigger unit** CX1172 to control grid is composed of two diodes connected in antiseries on input, with V_{BD}=1.5kV$_{RRM}$, that clamps spikes from grid, during thyratron commutation, dissipated on termination resistor R_X, antiinductive, type RCH25 47Ω/4W/700V$_{DC}$/1500V$_{FSM}$. In series to control pulse path there's D_X, a fast recovery diode type BYV79E/TO220/150V$_{RRM}$/14A$_{AVE}$/30ns$_{Trr}$ that has shown a reverse breakdown voltage just equal to negative bias of control grid, so no current is absorbed from input trigger unit. This configuration realizes a **DC coupling** between trigger unit and thyratron, avoiding dangerous time constant. Diodes and resistances are lie down on a hand made extruded heat sink.

Power supplies of cathode and reservoir drive filament resistances respectively R_k=0.18Ω and R_r=0.9Ω with a voltage about 6V$_{AC/DC}$. Cathode supply is ground referred and its positive output is ground for reservoir supply. **Two power transformers** are needed and are obtained from an unused analogous circuit with filaments supplied in AC. Cathode needs good heating with respect to reservoir, so lower resistance output transformer is chosen: with two loads and supposing a real model of generator, experimental estimation of output resistance results:

$$R_o = \frac{V_2 - V_1}{\frac{V_1}{R_1} - \frac{V_2}{R_2}} = \begin{cases} R_{o_R} = 22\text{m}\Omega \\ R_{o_K} = 10.35\text{m}\Omega \end{cases}. \tag{40}$$

In together case has been realized full wave rectifier for obtaining lower value of filter capacitor and diodes pulse current, higher value of output mean voltage (a little penalized by additional diodes drop voltage). **Reservoir power supply** provides following performances, with n=2 and electrolytic capacitance C$_{R1}$=68 000μF/ESR=20mΩ:

$$\begin{array}{ll} V_m = 6.9\text{V} & I_{d_p} = 44.2\text{A} \\ V_r = 0.6\text{V} & V_{D_R} \le 1.1\text{V} \\ I_{d_m} = 8\text{A} \equiv I_{\text{Reservoir}} & \end{array} . \tag{41}$$

Graetz diode bridge is GBPC35005/50V/35A_{AVE}/400A_{FSM}, then an additional lower filter electrolytic capacitance C_{R2}=2 200μF with lower parasitic inductance, finally a big protection varistor type SIOV-S20K14 of 18V_{DC}/12J/0.2W.

Cathode supply voltage has a discrete Graetz bridge realized by single, low V_F, Schottky diodes fixed on a big heat sink; then, follows a LC filter needed for reducing diodes pulse currents and harmonic spurious spectra of filament and supply absorbed currents.

It provides following design and experimental performances, with $n = 2$, C_{K1}=150000μF/ESR=8mΩ , power inductance L_K=73.15μH/ESR=1.71mΩ:

$$\begin{array}{l} V_m = 6.48\text{V} \\ V_r = 1.07\text{V} \\ I_{d_m} = 36.8\text{A} \equiv I_{\text{cathode}} \\ I_{d_p} = 220\text{A} \\ V_{D_{schottky}} \le 0.59\text{V}. \end{array} \tag{42}$$

The bridge is realized with double diodes, common cathode, in a single package, type 40CPQ045/45V_{RRPM}/40A_{AVE}/400A_{FSM} that have been connected in parallel with proper wire equilibrating resistors as shown in following picture:

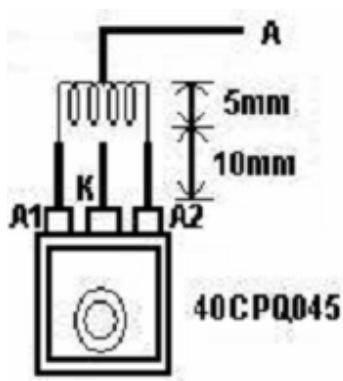

Fig. 21 − Generic full wave GRAETZ Schottky diode rectifier for cathode supply with equilibrating small value resistors realized by copper coil; center tap realizes anode connection. Silicone paste is used to guarantee low thermal resistance between case and heat sink. Mica foil accomplices insulation of each cathode respect to aluminum heat sink.

Then there is an additional lower filter electrolytic capacitance C_{K2}=2 200μF with lower parasitic inductance, finally a big protection varistor type SIOV-S20K14 of 18V_{DC}/12J/0.2W. Inductance L_K is designed under critic value, beyond which there is discontinue conduction on rectifier and diodes pulse current overcomes double of average current delivered to load:

$$L_{crit.} = 186.8\mu\text{H} > L_K = 73.15\mu\text{H} . \tag{43}$$

So, we obtain a higher output average filament voltage. Realization of L_K has needed 12 turns wounded on the biggest ferrite core type PM114/93, using flexible 25mm^2 cable type of heart grounding. All diodes have been SPICE modeled by starting to characteristic V_{AK}(@I_{A}) provided by supplier.

Thermal resistances have been obtained for all heat sink designing. Principal biasing PCB is taken **away from thyratron** by long and big wires for reducing electromagnetic interference generated with commutation and hard X-rays emitted from 33.5kV thyratron discharge.

3.3.3. Heat sinks for electronic devices

We have designed boards able to dissipate **directly in air** generated heat without oil aid, where they are dipped.

To obtain this result, it is necessary to design suitable heat sinks for components, also considering thermal resistances of silicone pastes and insulating films. So, **four Al extruded heat sinks,** with thickness of 1mm not painted, have been realized; design is based on: 1) determination of power dissipated from component; 2) verification that it is not yet able to dissipate this power; 3) from theoretical model, estimation of necessary thermal resistance of heat sink-environment; 4) the use of **nomogram** to calculate heat sink area.

By electric scheme, representing heat dissipation circuit of electronic components, it is possible to calculate $R_{\theta_{d-a}}$ **of heat sink-environment**. So, $R_{\theta_{d-a}}$ is obtained by using the following relation:

$$R_{\theta_{d-a}} = \frac{T_j - T_a}{P_d} - R_{\theta_{j-c}} - R_{\theta_{c-d}} \qquad \left[\frac{\text{K}}{\text{W}}\right]. \tag{44}$$

Two **clipping diodes** (D_{x1} and D_{x2}), put at input of control pulse, dissipate power (P_d =120mW @ maximum PRR of 350Hz) when they go to conduct ($I_{G2} \cong 11$A due to terminating resistance R_x=47Ω) through return grid spike of about 2kV/20ns due to thyratron commutation; the value of dissipated power, P_d, doesn't need necessarily heat sink, because diodes case is TO-220 that has $R_{\theta_{d-a}} < 4.7\,\text{K}/\text{W}$; however, for safety and mechanical reasons, we have realized a heat sink with area of 18cm^2, that connects cathodes of two clipping diodes without conductive pastes for heat.

Terminating resistance, R_x, dissipates power (P_d =2.3W) because of conduction current of control grid (I_{Gon}≅10A) and recovery one (I_{Goff}≅−2.3A). By using silicone paste ($R_{\theta_{c-d}} = 0.12\,\mathrm{K/W}$) and data sheet (for particular values of dissipated power and $R_{\theta_{d-a}}$, one obtains $R_{\theta_{j-c}} = 2.88\,\mathrm{K/W}$), one has $R_{\theta_{d-a}} = 8\,\mathrm{K/W}$; consequently, a heat sink with area of 40cm^2 is necessary.

Decoupling diode, D_x, dissipates power (P_d=1.8W) when in control grid circulates current (I_{G2}=11A) and when there are differences (of 15% for example) between breakdown inverse voltage (V_{BD}=−150V) and grid biasing inverse voltage (V_{G2}=−150V), that cause current conduction towards biasing resistors ($R_{b1,2}$); so, a heat sink with area of 50cm^2 is requested, if one uses mica as insulating material with $R_{\theta_{c-d}} = 1\,\mathrm{K/W}$.

Metal can resistor, R_p, dissipates continue power of 38W, so it needs three small heat sink plates with area equal to 64cm^2 to form Al layer 3mm thick.

Diode bridge of reservoir power supply dissipates power ($P_{d_{bridge}}$) 4 times higher than power dissipated from single diode, that is given by multiplication between direct drop voltage, V_f, and diode mean current, I_{dm}, that is:

$$P_{d_{bridge}} = \frac{4}{T} \cdot \int_{t_1}^{t_2} V_f \cdot i_{d_{1,3}}(t)\,dt = 4 \cdot V_f I_{dm} = 2 \cdot V_f I_{dc}\,, \tag{45}$$

where $i_{d_{1,3}}(t)$ is current of diodes 1 and 3 and I_{dc}=2I_{dm}. So, during time, only two diodes lead mean current (I_{dc}) of load and, consequently, they decide value of $P_{d_{bridge}}$, that in our case is equal to 16.2W.

Consequently, by using manufacturer diagrams, one obtains $R_{\theta_{j-c}} = 3.3\,\mathrm{K/W}$ and, thanks to silicone paste, one concludes that $R_{\theta_{d-a}} = 0.975\,\mathrm{K/W}$, realizable through heat sink with length equal to 18cm (Fig. 22).

Schottky diodes of cathode power supply bridge dissipate power ($P_{d_{schottky}}$) that is given by multiplication between direct drop voltage, V_f, and diode mean current, I_{dm}, that is:

$$P_{d_{schottky}} = \frac{1}{T} \cdot \int_{t_1}^{t_2} V_f \cdot i_d(t)\,dt = V_f I_{dm} = V_f \frac{I_{dc}}{2}\,, \tag{46}$$

where $i_d(t)$ is diode current. So, during time, each diode leads current equal to half value of load mean current (I_{dc}) and, in our case, one has $P_{d_{schottky}}$ = 8.4W.

Consequently, by using manufacturer diagrams, one obtains $R_{\theta_{j-c}} \cong 1\,\mathrm{K/W}$ and, thanks to silicone paste + mica ($R_{\theta_{c-d}} = 0.7\,\mathrm{K/W}$), one concludes that $R_{\theta_{d-a}} = 4.2\,\mathrm{K/W}$,

realizable through heat sink with length equal to 19cm (Fig. 22). Moreover, **all heat sinks have been connected to ground potential**, given by steel structure of main discharge circuit.

Concluding, in the next figure nomogram is reported; one begins from the right bottom with expected value of $R_{\theta_{d-a}}$, intercepting straight line corresponding to considered heat sink and to absolute vertical or horizontal position; from this point, one goes up intercepting straight line corresponding to power that one wants to dissipate. Then, one goes on the left intercepting straight line corresponding to used thickness; finally, one goes down intercepting curve corresponding to case of considered electronic component: the ordinate of this point gives heat sink area.

The result is valid for maximum length-height ratio equal to **1.25.**

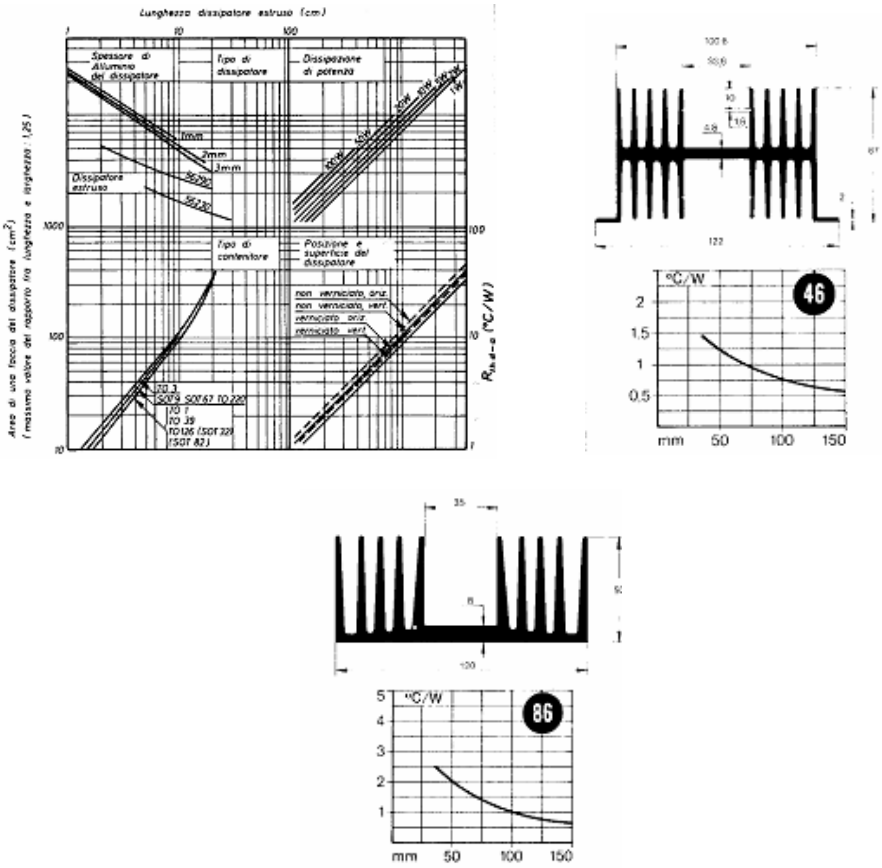

Fig. 22 − On the top left: nomogram to calculate extruded heat sink area. On the top right: scheme of n.46 standard heat sink, with chosen length equal to 18cm. On the bottom center: scheme of n.86 standard heat sink, with chosen length equal to 19cm.

3.3.4. Power inductor realization

Dimensioning of power inductor (or transformer) is necessary because its ferromagnetic core has a saturation magnetic field, B_{sat}, that imposes a **maximum limit value** to H_{sat} (remember that $H_{sat}=B_{sat}/\mu$, where μ is magnetic permeability of considered material), and, consequently, to inductor current before saturation phenomenon appears, that is (note that N is turns number, g indicates a gap of insulating material, as air, and $\mu_e(g)$ is effective magnetic permeability of ferromagnetic core circuit):

$$I_{\max} = \frac{B_{sat}}{N \cdot \mu_e(g)} . \tag{47}$$

Since gap, g, causes a reduction of core magnetic permeability through inversely proportional relation (while B_{sat} of core remains constant and, so, H_{sat} increases, Fig. 23), its presence produces an increase of saturation maximum current (I_{max}) of inductor and a small increase of N and, consequently, of Cu parasitic resistance, as one can see thanks to following relation, where L is auto-induction coefficient, A_e, l_e and $A_L(g)$ are effective area, length of core and **inductance factor**, due to complicate geometry of real magnetic circuit, given by manufacturer [2]:

$$L = \mu_e(g) \cdot N^2 \frac{A_e}{l_e} \cong N^2 \cdot A_L(g), \qquad \text{where} \qquad A_L(g) = k_1 \cdot g^{k_2}, \tag{48}$$

where k_1 and k_2 can be calculated by using two values of $A_L(g)$, given by manufacturer for two different gap values (g_1 and g_2), that is:

$$k_1 = \frac{A_L(g)}{g^{k_2}}, \qquad k_2 = \frac{\ln \frac{A_L(g_1)}{A_L(g_2)}}{\ln \frac{g_1}{g_2}}. \tag{49}$$

So, useful analytical expression to determine I_{max} is the following (remember always to verify that $l_L(t)<I_{max}$, where $I_L(t)$ is power inductor current):

$$I_{max}(g) = \frac{B_{sat} \cdot A_e}{N \cdot A_L(g)} . \tag{50}$$

Really, when approximately linear behavior of ferromagnetic core of power inductor (or transformer) is requested, it is necessary that $\boldsymbol{I_L<I_{10\%}}$, where $I_{10\%}$ is given by manufacturer and represents current value for which effective magnetic

permeability, $\mu_e(g)$, reduces its value of 10% respect to situation where one works with small currents.

Thanks to our experiences, one obtains approximately:

$$I_{10\%} = \begin{cases} \frac{1}{2} I_{\max} & g = 0 \\ \frac{2}{3} I_{\max} & g = n \cdot 0.1\text{mm}. \\ \frac{5}{6} I_{\max} & g = n \cdot 1\text{mm} \end{cases} \tag{51}$$

Finally, in Fig. 23 an example of hysteresis cycle for ferromagnetic core of power inductor is showed in two different cases: 1) without air gap; 2) with air gap. Our power inductor L_K=73μH has been realized through 12 turns of cable with section equal to 25mm^2.

Gap (g=5mm) is realized by tire O-ring, with diameter of 2.5mm, that separates first half core from second one, having dimensions of 2.5mm *each*, considering two branches of magnetic circuits: internal and external.

Concluding, in our case, one obtains:

$$I_L(\max) = 94\text{A} < I_{10\%} = 128\text{A} \leq I_{\text{sat}} = = 141\text{A}.$$

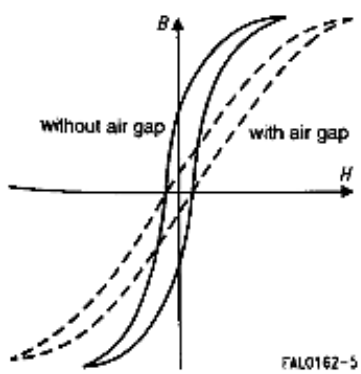

Fig. 23 − Hysteresis cycle for ferromagnetic core of power inductor in two different cases: 1) without air gap; 2) with air gap. Note that H_{sat} (and so I_{sat}) increases thanks to air gap introduction, with a moderate increase in number of turns.

3.4. MDC INTERFACES, PERFORMANCES AND FUTURE IMPROVEMENTS

In the steel structure that contains main electrical discharge circuit, various screwing holes have been realized. To begin, one considers high voltage teflon isolator connector, characterized by high dielectric rigidity that permits the use of

high supply voltage (33.5kV); then, one finds high voltage panel BNC connector that allows connection to CX1172 module of thyratron trigger for main discharge. Finally, one finds a big military connector with 24 pins to give 220V/50Hz to various internal power supplies.

Moreover, the cable arrives to 24 pin connector with length of 6m and contains 13 wires of section equal to 1.5mm^2 having twisted configuration; it is connected to ***rack module*** for controlling of main discharge circuit. Four of 13 wires are connected to two thermostats put inside main discharge circuit, that release and switch-off all power supplies of thyratron when temperature is higher than **55−60°C**, realizing an Automatic Thermal Protection (PAT).

However, it is possible to disable PAT and, consequently, protect by electric network fuse; in addition, one can disable reservoir power supply of thyratron, particular when thyratron is young. It is also interesting that every command of rack module has a spy light. Concluding, Fig. 24 represents the electric scheme of command rack module.

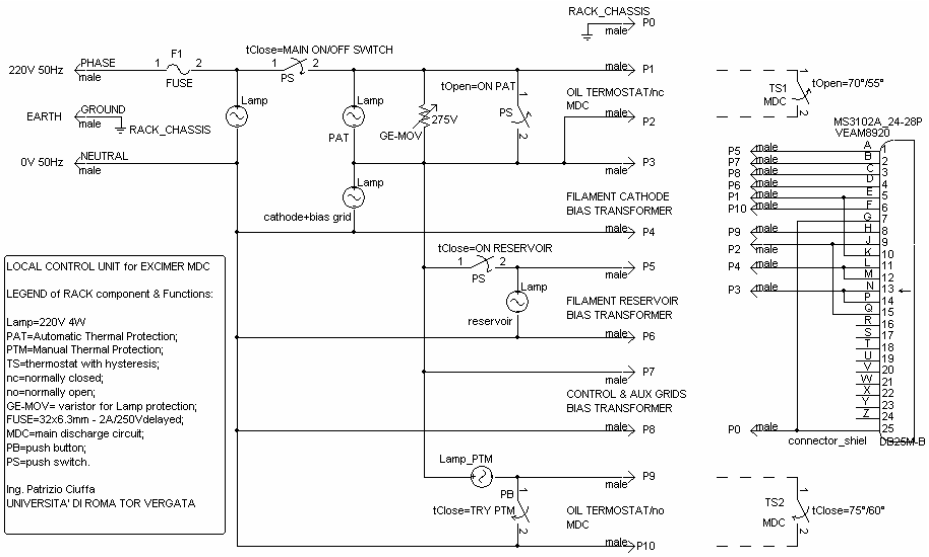

Fig. 24 − Electric scheme of command rack module LCU for Main Discharge Circuit.

3.4.1. Measurement of DC-priming biasing voltages

Following figures report three graphs concerning some measures of *DC-priming* biasing voltages. In particular, in Fig. 25, graph concerning cathode filament biasing voltage versus time; in Fig. 26, graph relative to negative bias

voltage of thyratron control grid versus time; finally, in Fig. 27, graph concerning auxiliary grid bias voltage during thyratron heating.

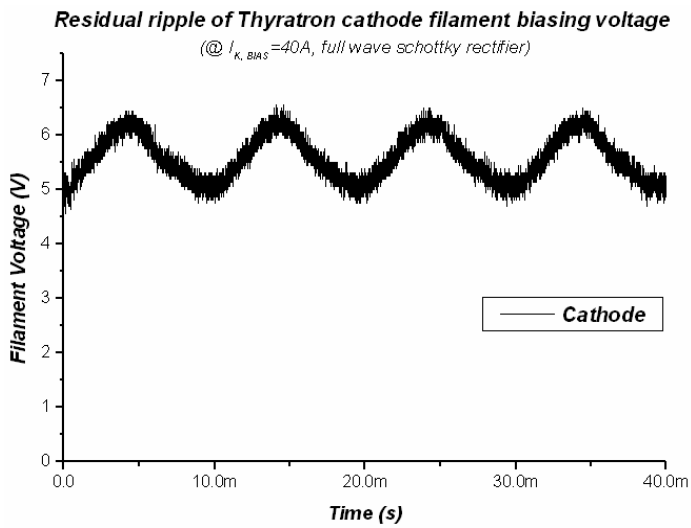

Fig. 25 − Some measurements of DC-priming biasing voltages versus time concerning thyratron cathode filament. Note that some working conditions are reported directly in the graph.

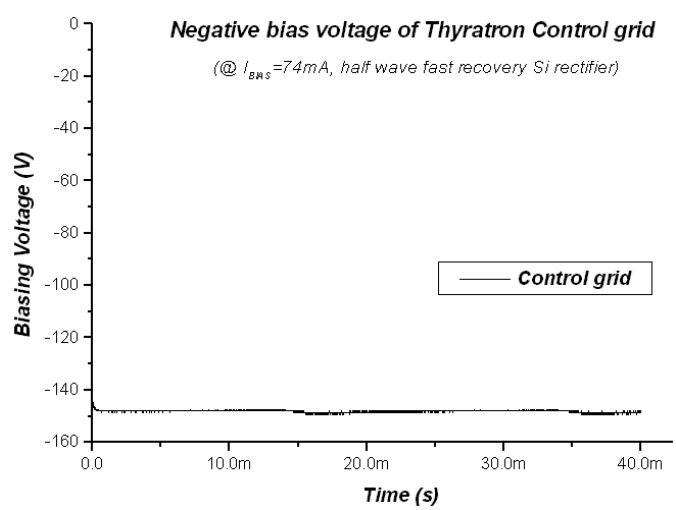

Fig. 26 − Some measurements of DC-priming biasing voltages versus time concerning thyratron control grid. Note that some working conditions are reported directly in the graph.

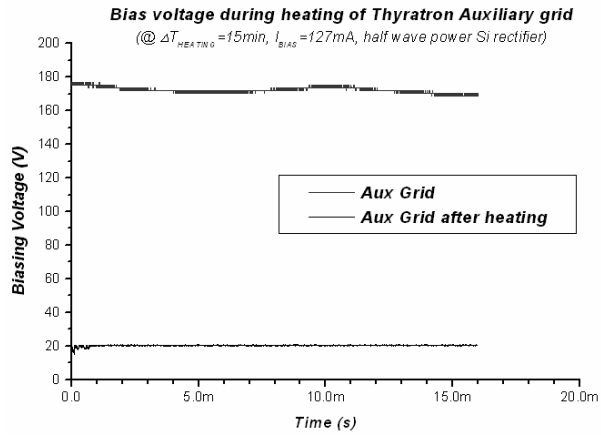

Fig. 27 − Some measurements of DC-priming biasing voltages versus time concerning thyratron auxiliary grid. Note that some working conditions are reported directly in the graph.

3.4.2. Discharge experiments

In the next first figure, graph represents main discharge voltage at laser electrodes versus time during thyratron commutation with HVPS voltage of 15kV; this graph shows supply voltage inversion around −27.5kV due to ***LC-inversion*** configuration and consequent exponential damping with some oscillations due to spurious inductance of discharge electrodes (about 30nH) and, mainly, to discharge gaseous mixture.

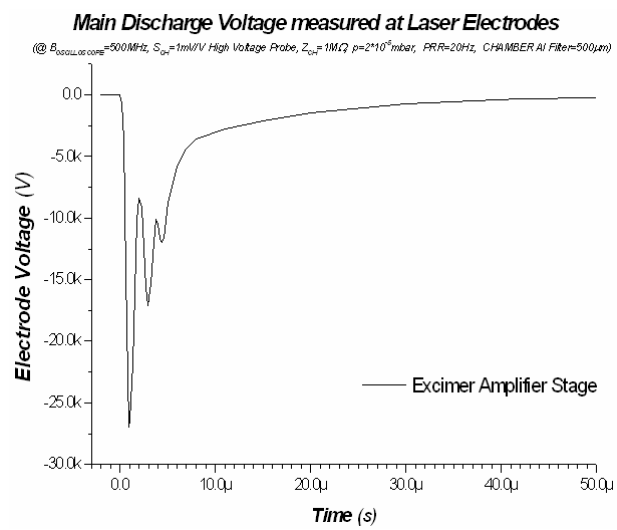

Fig. 28 − Main discharge voltage measured at laser electrodes versus time @ HVPS=15kV.

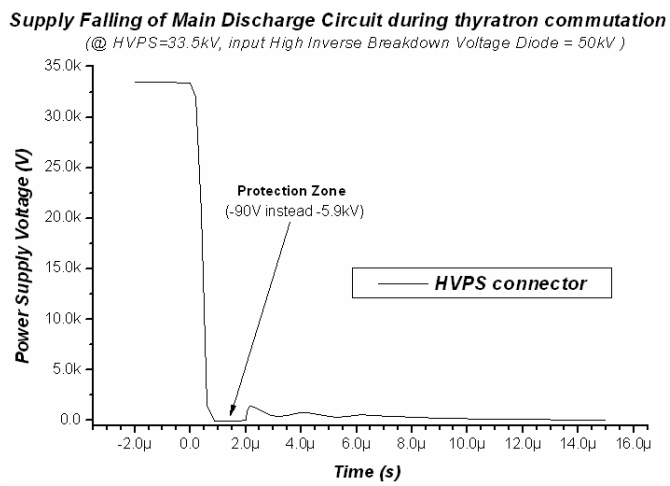

Fig. 29 − Power supply voltage versus time @ HVPS=33.5kV.

In Fig. 29, graph shows temporal behavior of power supply voltage HVPS = 33.5kV, measured at input connector, during thyratron commutation when main discharge happens and diodes of protection input circuit go to conduct; protection value of −90V is showed on the graph, according to −84V obtained from SPICE simulations. Moreover, we have made 14 measures concerning temporal delay, Δt, between rise front of thyratron command pulse and successive fall front due to thyratron anode commutation.

Finally, measured standard deviation of Δt gives commutation jitter of main discharge circuit, that is:

$$E\{\Delta t\} = \overline{\Delta t} = 65.41\text{ns}, \qquad jitter_{MD} \cong \sigma_{\Delta t} = E\left\{\left|\Delta t - \overline{\Delta t}\right|\right\} = 0.5\text{ns}. \tag{52}$$

Obtained value is **0.5ns**, that is limit value for performances of our thyratron; this is possible thanks to particular method of continue biasing ***(DC-priming)***.

4. CONCLUSIONS

Experiments of X spectroscopy and microscopy are carrying out in the range of wavelengths around 1nm (soft X-rays) from laser induced plasma. So, we are working to a possibility to realize systems for generation of soft X radiation by dense and hot plasmas, produced through high intensity pulsed tabletop laser (as Tor Vergata *ns/infrared* laser source, or Tor Vergata ultrashort *fs/ultraviolet* laser source) focused with micrometric spot on metallic targets.

After an intense research activity, end amplifier stage unit of Tor Vergata ultrashort *fs* Ti:Sa laser system, based on KrF Excimer laser (λ=248nm, *UV* radiation, pulse energy E=0.1J, Pulse Repetition Rate =100Hz), has been developed, tested alone and not yet integrated in the laser system. Discharge test measurements, concerning preionizer module, have been executed: in particular, has been measured preionizer hard X energy versus its anode voltage.

Has been designed and realized the Main Discharge Circuit (MDC) necessary to supply the mixture main discharge after preionizing; this high power circuit is based on gas switch (thyratron) that a match high voltage range with ease to be on/off driven. Then, the best commutation performances have been reached by DC biasing and coupling of all thyratron grids.

All polarization voltages of thyratron grids have been verified, considering static and dynamic regimes; moreover, entire discharge tests have been executed and the effectiveness of trigger input protection circuit has been verified. In addition, has been demonstrated the effectiveness of protection circuit for high voltage DC supply input of MDC, even if reliability has to improve.

All high power components are cooled by aluminum heat sink, properly designed for working in ambient air at maximum PRR, even if entire MDC is installed in a stainless still container filled by oil that makes several functions: increase of the dielectric rigidity of discharge capacitors surrounding material and cooling MDC by an external recirculation pump.

Finally, minimum commutation jitter of main discharge circuit of Excimer amplifier stage has been demonstrated, by implementing of thyratron DC biasing and DC coupling of triggering pulse (*DC-priming* technique).

Also, has been described the High Voltage Power Supply (HVPS) stage for MDC, the HVPS stage for preionizer cathode and the HVPS stage for preionizer anode: all these three HVPS stages are synchronized with MDC by a *DELAY MANAGEMENT MODULE* designed in Tor Vergata University and realized by ELSON srl.

The rack command module, designed and realized in Tor Vergata University, makes the function of main machine interface for switching on/off and thermal protection of entire Excimer amplifier unit.

We will complete experimental setup of ***Tor Vergata UV ultrashort pulsed laser system*** by integration of *KrF Excimer laser end amplification* unit, *compressor* unit and *vacuum chamber* unit for plasma X-ray generation, in agreement to scheme reported previously (CPA technique and MPA architecture).

Moreover, in alternative to Tor Vergata Nd:Yag/Glass laser source, we will use our *UV fs ultrashort pulsed laser system* to produce plasmas on targets through ultrahigh laser intensities. So, we expect to reach laser intensities on target of the order of 10^{16}W/cm^2 at least and conversion efficiencies from *UV* radiation to X-rays of about 10%.

Concluding, for the future, we are designing to make first laser micromachining of photoresist structures, as silicon wafer (dimension=4 inches) with 400nm thick PMMA layer deposited on Si surface, for executing **first our microlithography experiments**.

REFERENCES

1. P. Ciuffa, *Sistemi per la Generazione e Rivelazione di Raggi X da Plasma Indotto da Laser, per applicazioni di Microlitografia, Radiobiologia, Microscopia*, PhD Thesis of Microsystem Engineering, XIII Cycle, University of Rome "Tor Vergata", Engineering Faculty, Department of "Ingegneria dell'Impresa" (ex "Scienze e Tecnologie Fisiche ed Energetiche), Academic Year 1999–2000.
2. ** Siemens Matsushita Components, *Ferrites and Accessories*, Data book (1997).